Hindawi
Advances in Meteorology
Volume 2024, Article ID 9927285, 12 pages
https://doi.org/10.1155/2024/9927285

Research Article

Application of wetPf2 Data for Investigating Characteristics of Temperature and Humidity of Air Masses over Paracel and Spratly Islands

Khuong Le Pham[1,2] **Anh Xuan Nguyen**[1,2] **Hiep Van Nguyen**[1,3] **Son Hai Hoang**[1,2] **Vinh Nhu Nguyen**[1,2] **and Thang Van Vu**[4]

[1]*Institute of Geophysics, Vietnam Academy of Science and Technology, Hanoi, Vietnam*
[2]*Graduate University of Science and Technology, Vietnam Academy of Science and Technology, Hanoi, Vietnam*
[3]*Northern Delta and Midland Regional Hydro-Meteorological Center, Vietnam Meteorological and Hydrological Administration, Hanoi, Vietnam*
[4]*Vietnam Institute of Meteorology, Hydrology and Climate Change, Hanoi, Vietnam*

Correspondence should be addressed to Hiep Van Nguyen; hiepwork@gmail.com

Received 7 August 2023; Revised 9 January 2024; Accepted 6 February 2024; Published 28 February 2024

Academic Editor: Nicholas Meskhidze

This article uses data from the second-generation Constellation Observing System for Meteorology, Ionosphere, and Climate (COSMIC-2) satellites (wetPf2) to study the temperature and humidity properties of the air masses over Paracel and Spratly Islands in the Vietnam East Sea (South China Sea). The satellite observational data were validated with the radiosonde data from three stations in Vietnam: Hanoi, Danang, and Ho Chi Minh City. Subsequently, the wetPf2 data are used to analyze the characteristics of temperature and relative humidity variations of the air masses over the Paracel and Spratly regions. Results show that the mean error of the satellite observational data for temperature ranges from −0.06°C to −0.02°C, with standard deviations ranging from 0.73°C to 1.04°C. The mean error of relative humidity fluctuates between 11.6% and 12.5%, with standard deviations ranging from 15.1% to 19.1%. The values are reasonable and comparable to those in previous studies. Seasonal variations of temperature and humidity show that the air mass over the Paracel Islands exhibits a larger annual temperature with an annual variation of approximately 5.0°C, significantly higher than the value of 2.2°C in the air mass over the Spratly Islands. The difference may be due to the greater influence of continental and seasonal wind systems in the northern region. Within both air masses, the annual temperature variation in the boundary layer is much larger than that in the free atmosphere. Annual relative humidity variation is higher in summer and autumn than in winter and spring. The significant changes in the relative humidity with height during winter and no significant change of the relative humidity with height during summer may be related to the important role of strong convective activity carrying moist air upward to higher atmospheric levels during the summer time.

1. Introduction

Observational data from traditional monitoring stations (surface and radiosonde stations) are mainly located on land. Researching the characteristics of atmospheric masses in maritime areas faces many difficulties due to the lack of data. With the development of remote sensing techniques, satellites enable measurements and estimation of temperature and humidity profiles of atmospheric masses over the ocean, where traditional observational data are scarce. The Radio Occultation (RO) technique uses signals emitted by the Global Positioning System (GPS) satellites to monitor the Earth's atmosphere. This technique was first used in the GPS/MET (GPS Meteorology) project [1]. Subsequently, the RO technique was further developed and improved by Kursinski and colleagues [2]. Today, this technique has been employed in many projects [3–8]. The projects have provided a large volume of Global Positioning System Radio

Occultation (GPSRO) data on a global scale. GPSRO data are an important source of atmospheric profile survey data, particularly in regions without conventional radiosonde monitoring stations, such as over the open oceans and polar regions.

Many authors have evaluated the quality of GPSRO data. GPSRO data are often evaluated by comparing one or several meteorological fields of GPSRO data with radiosonde data. Previous studies suggested that the temperature profile data from FORMOSAT-3 (Formosa Satellite 3) are consistent with that of radiosonde data in the Australian region [9, 10]. Over China region, the average temperature difference was about −0.10 K, and the RMSE error was 4.84 K in the 0–40 km layer [11]. Globally, the temperature profiles observed by the Constellation Observing System for Meteorology, Ionosphere, and Climate (COSMIC) agree well with those obtained from most types of radiosondes [12, 13]. Regarding relative humidity profiles, GPSRO data tends to be drier compared to radiosonde data, especially in the upper troposphere, where the mean error can reach 5–8% [12]. Evaluation results of COSMIC-2/FORMOSAT-7 data show that the average temperature difference between COSMIC-2 and radiosonde in the 8–30 km layer is about −0.04 K, with a standard deviation of 1.34 K. The temperature profile of COSMIC-2 in lower stratosphere is highly accurate when compared to radiosonde data [14]. Another study showed corresponding mean errors and standard deviations of 0.22 K and 0.95 K (in the 8 km–11 km layer) and 0.00 K and 1.10 K (in the 12.5 km–16.5 km layer) [15]. For relative humidity, in the Asian monsoon region, the mean errors and standard deviations are 10% and 15%–20%, respectively [16].

In addition to quality assessment, GPSRO data has also been used to study and analyze the variations of meteorological variables. The COSMIC-2/FORMOSAT-7 project, a collaborative effort between Taiwan and the United States, uses low-Earth orbit satellites for atmospheric monitoring and measurement. These satellites collectively provide 5000 soundings per day worldwide [8]. The wetPf2 (atmospheric profiles of refractivity, temperature, and water vapor) data from COSMIC-2/FORMOSAT-7 provides vertical profiles of temperature, pressure, water vapor pressure, refractivity index, and relative humidity. The vertical resolution of this data is 50 m below 20 km altitude and 100 m at higher altitudes. The COSMIC-2/FORMOSAT-7 data have been used to analyze the variations in total precipitable water (TPW) in the East Sea and the Bay of Bengal. The results show that the wetPf2 data are in good agreement with the analysis from CFSR data and simulations from WRF [17].

Currently, in Vietnam, there are radiosonde monitoring stations located in Hanoi, Da Nang, and Ho Chi Minh City that perform measurements twice a day. The use of satellite remote sensing data has significant potential in atmospheric research and operational weather forecasting. RO data have also been used to experimentally assimilate into numerical models for rainfall forecasting in the Southern region of Vietnam [18]. From October 2019, the COSMIC-2/FORMOSAT-7 project has provided a large amount of wetPf2 data in the Vietnam region. This is a valuable data source that helps enhance the spatial and temporal density of temperature and humidity profile data in the Vietnam region, particularly in the East Sea, where there are no monitoring radiosonde stations.

The wetPf2 data show good quality in other regions of the world. To enhance the effectiveness of using this data over the Vietnam region, it is necessary to evaluate the quality of the wetPf2 data by comparing them with Vietnam radiosonde observations. Since radiosonde stations are not available over the East Sea, detailed investigations of the temporal and spatial variations in the characteristics of air masses over the region have not been conducted using observed data. After quality assessment, the wetPf2 data can be employed to study the characteristics of atmospheric fields over the East Sea region.

This article firstly assesses the quality of wetPf2 data in the Vietnam region. The temperature and relative humidity profiles of wetPf2 data are compared with radiosonde observations (RAOB) data in Hanoi, Da Nang, and Tan Son Hoa (Ho Chi Minh City). The evaluated data are then used to study the characteristics of temperature and humidity variations with height and season for air masses in the Paracel Islands, representing the northern air mass of the East Sea, and in the Spratly Islands, representing the southern air mass of the East Sea. The subsequent sections of the article include: Section 2 shows data and method, which outlines the data sources and calculation methods, and evaluates the data quality; Section 3 presents the main findings of the article, analyzes the data quality, and the characteristics of temperature and humidity variations in the studied maritime area; and a summary and discussion are given in Section 4.

2. Data and Methodology

2.1. Data. This study utilizes wetPf2 data (COSMIC-2/FORMOSAT-7) from the Central Weather Administration (CWA) during a period of 4 years from October 2019 to September 2023 (https://tacc.cwa.gov.tw/data-service/fs7rt_tdpc/daily_tar/). The wetPf2 data includes vertical profiles of temperature and relative humidity at a vertical resolution of 50 m. Radiosonde data (RAOB) for the same period are from three radiosonde stations in Vietnam, namely Hanoi (21.01°N 105.80°E), Da Nang (16.03°N 108.20°E), and Tan Son Hoa (Ho Chi Minh City) (10.81°N 106.66°E). The RAOB data are obtained from the University of Wyoming (https://weather.uwyo.edu/upperair/sounding.html). The 30 years of data (1991 to 2020) from the fifth generation of ECMWF (European Centre for Medium-Range Weather Forecasts) reanalysis, known as ERA5 (https://cds.climate.copernicus.eu), covering air temperature at the 2-meter level and winds at the 10-meter level from the ground, are utilized to calculate long-term climatological means for analyzing the annual variation in air-mass characteristics.

2.2. Method for Comparison between wetPf2 and Radiosonde Data. One of the most important steps in evaluating GPSRO data are the selection of corresponding pairs of GPSRO and RAOB data for comparison. Previous studies have proposed various criteria for selecting data pairs. These criteria take into account differences in distance and time between the two datasets such as differences of 100 km, 200 km, 300 km in distance, and 1 h, 2 h, 3 h in observed time [9]; differences of 100 km and 1 h [13]; differences of 25 km, 75 km, 125 km, 175 km, 225 km, 275 km, and 0.5 h, 1.5 h, 2.5 h, 3.5 h, 4.5 h, and 5.5 h [12]. In this work, we employ criteria involving maximum time differences of 1 h, 2 h, and 3 h, as well as maximum spatial differences of 100 km, 200 km, and 300 km to create nine groups (GP1 to GP9) of data for comparison and verification, as illustrated in Table 1.

After selecting the data pairs corresponding to the above data groups, the temperature and relative humidity data of wetPf2 were interpolated to the standard isopressure levels of 925 mb, 850 mb, 700 mb, 500 mb, 400 mb, 300 mb, 250 mb, 200 mb, 150 mb, and 100 mb [13].

$$T = \alpha . T_1 + \beta . T_2, \quad (1)$$

$$\mathrm{RH} = \alpha . \mathrm{RH}_1 + \beta . \mathrm{RH}_2, \quad (2)$$

$$\alpha = \frac{\ln P - \ln P_2}{\ln P_1 - \ln P_2}, \quad (3)$$

$$\beta = \frac{\ln P_1 - \ln P}{\ln P_1 - \ln P_2}, \quad (4)$$

where T and RH are temperature and relative humidity at pressure level P; $T1$, RH1 is the temperature and relative humidity at the pressure level $P1$; $T2$ is the temperature; and RH2 is the relative humidity at the pressure level $P2$.

Due to the significant variability of relative humidity or any moisture parameter in the troposphere, interpolating values between different levels, especially in the upper troposphere (e.g., 250 mb, 200 mb, 150 mb, 100 mb, or close to the tropopause), may introduce unwanted signals (or noise). Although unwanted signals are unavoidable, to minimize the noise, the very high vertical resolution (50 m interval) of GPSRO data is utilized. Applying the weighted interpolation method (equation (2)) for relative humidity interpolation in this dataset, with a maximum vertical interpolation distance of less than 50 m, may reduce unwanted signals.

The mean and standard deviation of the error between the RO and RAOB data were used for the evaluation.

$$\begin{aligned}
\Delta T &= T^W - T^R, \\
\Delta \mathrm{Tm} &= \frac{1}{n}\sum_{i=1}^{n} \Delta\left(T_i^W - T_i^R\right), \\
\Delta \mathrm{RH} &= \mathrm{RH}^W - \mathrm{RH}^R, \\
\Delta \mathrm{RHm} &= \frac{1}{n}\sum_{i=1}^{n} \Delta\left(\mathrm{RH}_i^W - \mathrm{RH}_i^R\right), \\
\mathrm{SD}_{\Delta T} &= \sqrt{\frac{1}{n}\sum_{i=1}^{n} \left(\Delta T_i - \Delta \mathrm{Tm}\right)^2}, \\
\mathrm{SD}_{\Delta \mathrm{RH}} &= \sqrt{\frac{1}{n}\sum_{i=1}^{n} \left(\Delta \mathrm{RH}_i - \Delta \mathrm{RHm}\right)^2}.
\end{aligned} \quad (5)$$

Table 1: Data groups for pair comparison.

Distance (km)	≤1 h difference	≤2 h difference	≤3 h difference
Distance ≤100	GP1	GP2	GP3
Distance ≤200	GP4	GP5	GP6
Distance ≤300	GP7	GP8	GP9

In which, T^W and RH^W are the temperature and relative humidity of the wetPf2 data; T^R and RH^R are the temperature and relative humidity of the RAOB data; ΔT and ΔRH are the differences in temperature and relative humidity between the wetPf2 data and the RAOB data; ΔTm and ΔRHm are the mean errors of temperature and relative humidity; $\mathrm{SD}_{\Delta T}$ and $\mathrm{SD}_{\Delta \mathrm{RH}}$ are the standard deviations of the temperature and relative humidity errors; n is the number of samples (pairs of data).

2.3. Method for Determining Characteristics of Meteorological Fields of Air Masses. From wetPf2 data, we calculated the average profile of temperature and relative humidity for air masses over the Paracel Islands (13°N–18°N, 110°E–115°E), Spratly Islands (7°N–12°N, 110°E–115°E), and the land (13°N–18°N, 101°E–106°E) regions (Figure 1).

The average gradient according to the altitude of the mean temperature ($\Delta \mathrm{Tm}(z_k)$) and relative humidity (ΔRHm (z_k)) at level k is calculated as follows:

$$\Delta \mathrm{Tm}\left(z_k\right) = \frac{1}{n}\sum_{\mathrm{i}=1}^{n} \left(T_{k,i}^W - T_{k+1,i}^W\right), \quad (6)$$

where $T_{k,i}^W$ and $T_{k+1,i}^W$ are the temperature at k and $k+1$ of the i^{th} temperature profile wetPf2 data, respectively; and n is the number of data.

3. Results

3.1. Evaluate Data Quality of wetPf2. Figure 2 presents the mean error values (ΔTm) and the standard deviation of temperature errors ($\mathrm{SD}_{\Delta T}$) between wetPf2 data and the radiosonde data at different altitudes corresponding to 9 groups of data. The values of ΔTm at all altitudes in all data groups range from −0.31°C to 0.12°C. At altitudes of 925 mb, 300 mb, 250 mb, and 200 mb, all ΔTm values are negative, indicating that the wetPf2 data generally have lower temperature values compared to the radiosonde data. The mean error values of the data groups range from −0.06°C to −0.02°C. The $\mathrm{SD}_{\Delta T}$ values at all altitudes are less than 1.7°C. The $\mathrm{SD}_{\Delta T}$ values decrease from 925 mb to 200 mb. At 200 mb, $\mathrm{SD}_{\Delta T}$ is the smallest, ranging from 0.42°C to 0.67°C. From 200 mb to 100 mb, the $\mathrm{SD}_{\Delta T}$ values increase gradually with average standard deviation values from 0.73°C to 1.04°C. The average standard deviation in the GP1 case is the smallest, with a value of 0.73°C. The average standard deviation in the GP9 case is the largest, with a value of 1.04°C (Figure 2). Previous studies reported a mean temperature difference of 0.22 K with a standard deviation of 0.95 K between wetPf2 data and RAOB data in the layer from 8 km to 11 km. In the layer from 12.5 km to 16.5 km, the mean temperature difference is zero with a standard deviation of

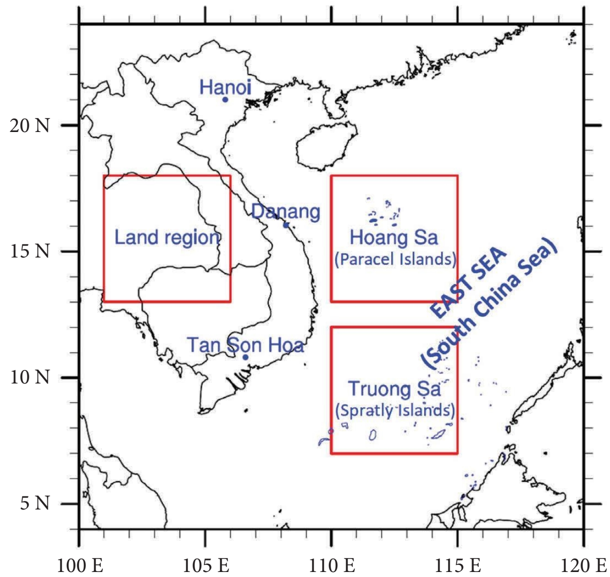

Figure 1: The study area and location radiosonde monitoring stations.

1.10 K [15]. Therefore, the calculated average temperature errors and standard deviations in the Vietnam and East Sea regions are reasonable.

Table 2 presents the correlation coefficient values (R (T)) of temperature between the wetPf2 data and the radiosonde data at each altitude level for the 9 data groups. The results show that the value of R (T) at all altitudes is equal to or greater than 0.78. At the 700 mb and 500 mb levels, the value of R (T) is lower than at other levels. The change in R (T) values with respect to time differences (one to three hours) is smaller than the change with respect to distances (100 km to 300 km) (Tables 1 and 2). The GP1 case has the highest average R (T) value (0.93), and the GP9 case has the lowest average R (T) value (0.86). This means that the wetPf2 data closer in time and distance to the radiosonde station observation have a better temperature correlation coefficient. The overall values of R (T) for all data groups indicate a good correlation between the temperature profile of wetPf2 data and radiosonde data.

Figure 3 presents the variations of the mean error and standard deviation of the error of relative humidity between the wetPf2 data and the radiosonde data at the corresponding altitude levels for the 9 data groups. Figure 3(a) illustrates the profile of the mean error of relative humidity (ΔRHm). The ΔRHm values below 400 mb are smaller compared to the values above 400 mb. The ΔRHm values at altitudes below 400 mb range from −5.6% to 4.6%. For altitudes above 400 mb, the ΔRHm values vary from 10.3% to 40.5%. The ΔRHm values do not differ significantly among the 9 data groups, with most differences being less than 2.7%. The average ΔRHm for all cases oscillates between 11.6% and 12.5%. In Figure 3(b), the variations of the standard deviation of the relative humidity error ($SD_{\Delta RH}$) are presented. The $SD_{\Delta RH}$ values are smaller at lower altitude levels compared to higher levels, and the maximum $SD_{\Delta RH}$ is observed at 250 mb and 200 mb for all data groups. The minimum value of $SD_{\Delta RH}$ is found at 925 mb. The smallest average $SD_{\Delta RH}$ occurs in case GP1 (15.1%), while the largest occurs in case GP9 (19.06%). The results also indicate that the difference in the value of $SD_{\Delta RH}$ with respect to time is smaller than the difference in the value of $SD_{\Delta RH}$ with respect to distance. Previous studies have shown that the mean error of relative humidity is about 10% with a standard deviation of 15% to 20% in the Asian monsoon region [16]. The mean error of relative humidity in this work ranges from 11.6% to 12.5% with a standard deviation of 15.1% to 19.1%, which is consistent with previous research results.

Figure 3(b) shows that the standard deviation of the humidity error is separated into three groups corresponding to the three groups of distance from the observation station: 100 km, 200 km, and 300 km. This suggests that the mean error (mean difference between satellite observation data and radiosonde observation data) contains three sources including (i) error due to satellite observation quality at the same location with the radiosonde observation station, (ii) difference in data due to temporal variations in the internal characteristics of the air mass (due to satellite observation time does not coincide with the observation time at the radiosonde station), and (iii) difference due to satellite observation and the spatial location of the radiosonde observation station in different air mass positions (Figure 3(b)). In the future, if a sufficiently long dataset becomes available for filtering satellite observation data and radiosonde observation data based on time and location, the errors in the dataset will solely come from the quality of satellite observations. This could potentially lead to a substantial reduction in overall differences compared to the errors present in the current dataset used in this study.

The correlation coefficient of relative humidity (R (RH)) between wetPf2 data and radiosonde data are presented for each altitude level of the 9 data groups in Table 3. The results indicate significant variation in the R (RH) values across altitudes and data groups. At altitudes of 925 mb and 850 mb, R (RH) values are relatively low, ranging from 0.43 to 0.70. For altitudes ranging from 700 mb to 250 mb, R (RH) exhibits higher values compared to other altitudes (R (RH) > 0.60). Notably, the maximum value of R (RH) is observed at the 500 mb altitude, ranging from 0.81 to 0.91, depending on the data group. At levels lower than 500 mb, active convection causes relative humidity (RH) to significantly change with space, resulting in more pronounced differences between RH data at radiosonde stations and satellite sample locations, especially at 925 mb level (Figure 3(a)). Figure 3(a) also shows that the mean error of RH at 500 mb is smaller than at lower levels. At levels higher than 500 mb, the amount of atmospheric moisture (mixing ratio) is relatively small, leading to a relatively larger RH error (Figure 3(a)). In addition, a larger number of samples at 500 mb (Figure 2) makes R (RH) statistics more robust. These factors may be important contributors to the correlation coefficient between the two data sources at the 500 mb level being the largest compared to the remaining levels. The average R (RH) value is highest for case GP1 (0.76) and lowest for case GP9 (0.63). A comparison between wetPf2 data and RAOB data have revealed that case GP1 yields the best results with

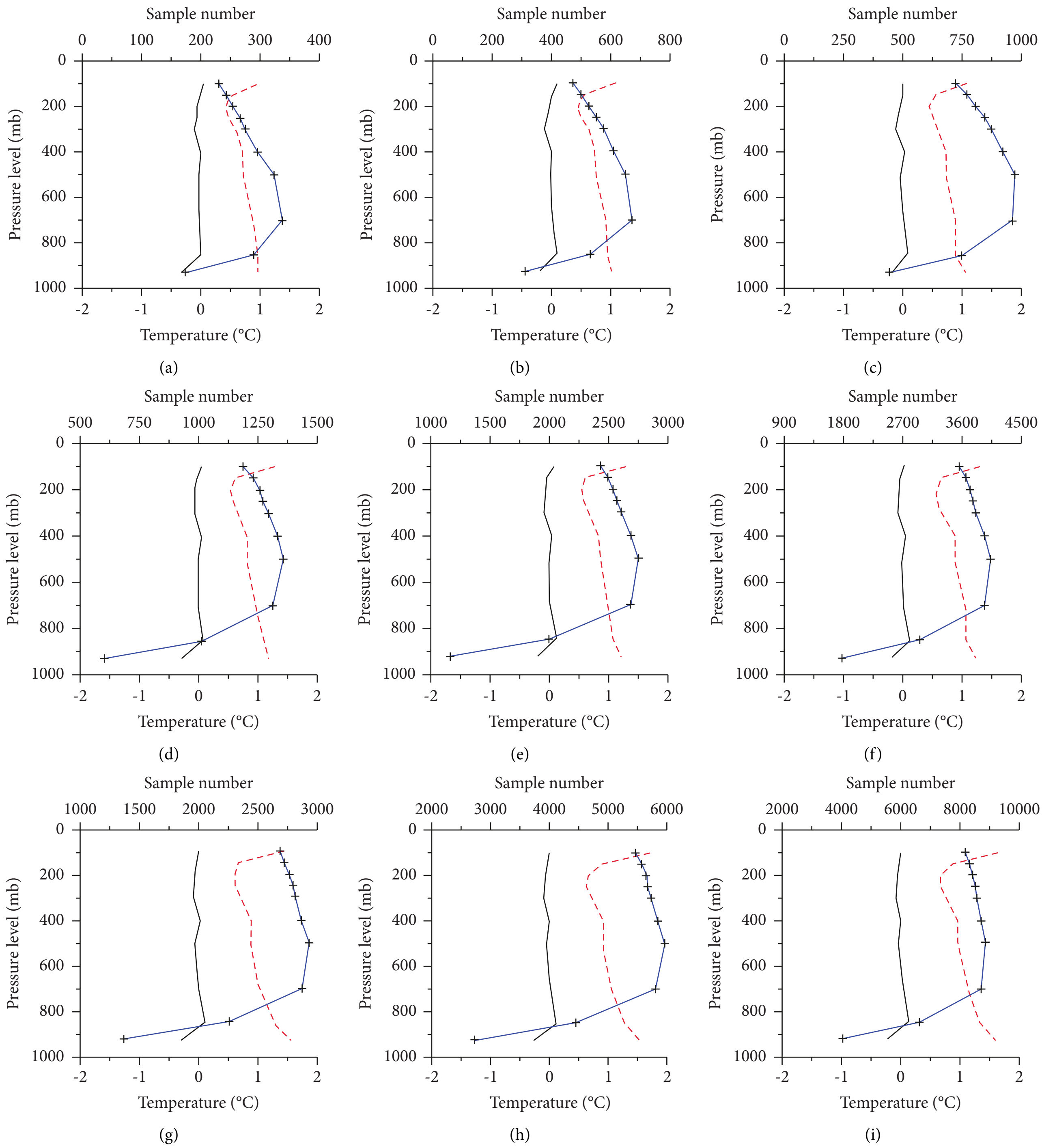

Figure 2: Mean error and standard deviation of temperature error calculated between wetPf2 data and radiosonde data at various altitudes. (a–i) correspond to data groups GP1, GP2, GP3, GP4, GP5, GP6, GP7, GP8, and GP9, respectively. The vertical axis denotes the barometric level, the lower horizontal axis indicates the temperature error value, and the upper horizontal axis represents the number of samples. The black solid line is the mean error value, the red dashed line illustrates the standard deviation of the error, and the blue solid (+) line indicates the number of samples.

the least number of available observations. Conversely, case GP9 produces the poorest results despite having a large number of available observations.

Overall, the mean error values, standard deviations, and average correlation coefficients between wetPf2 data and radiosonde data for both temperature and relative humidity

Table 2: Correlation coefficients of temperature between wetPf2 data and radiosonde data at each corresponding altitude level for each data group.

Pressure (mb)	GP1	GP2	GP3	GP4	GP5	GP6	GP7	GP8	GP9
925	0.97	0.97	0.96	0.94	0.94	0.93	0.89	0.90	0.89
850	0.96	0.96	0.96	0.94	0.95	0.94	0.91	0.91	0.91
700	0.89	0.88	0.88	0.87	0.86	0.83	0.84	0.83	0.80
500	0.87	0.87	0.87	0.87	0.85	0.83	0.84	0.82	0.81
400	0.90	0.88	0.88	0.90	0.88	0.87	0.86	0.85	0.84
300	0.93	0.92	0.93	0.92	0.91	0.92	0.90	0.89	0.89
250	0.96	0.95	0.95	0.94	0.93	0.93	0.92	0.92	0.91
200	0.96	0.96	0.95	0.94	0.93	0.93	0.91	0.90	0.90
150	0.93	0.94	0.93	0.92	0.92	0.91	0.89	0.84	0.85
100	0.91	0.91	0.90	0.87	0.86	0.85	0.83	0.78	0.79

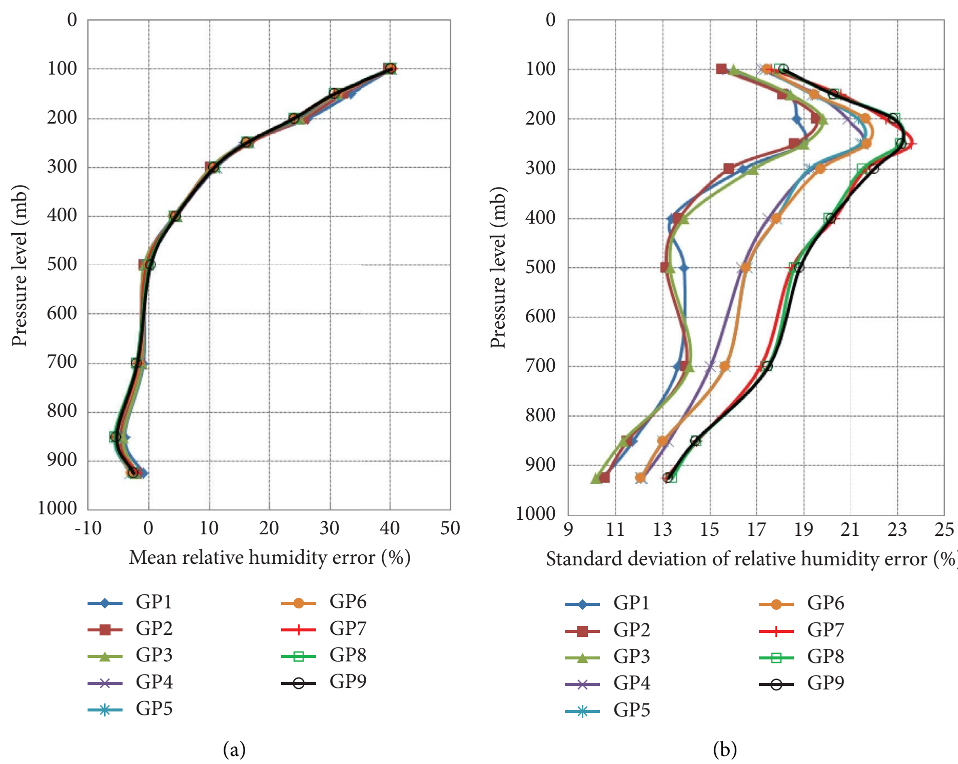

Figure 3: The mean error and standard deviation of the error in relative humidity between wetPf2 data and radiosonde data calculated for nine data groups at corresponding altitude levels for: (a) the mean error of relative humidity and (b) the standard deviation of the error of relative humidity.

Table 3: Correlation coefficients of relative humidity between wetPf2 data and radiosonde data at each altitude level for the 9 data groups.

Pressure (mb)	GP1	GP2	GP3	GP4	GP5	GP6	GP7	GP8	GP9
925	0.67	0.68	0.70	0.55	0.55	0.54	0.47	0.43	0.44
850	0.65	0.63	0.67	0.55	0.56	0.57	0.46	0.45	0.46
700	0.84	0.84	0.84	0.82	0.80	0.81	0.77	0.76	0.76
500	0.90	0.91	0.91	0.86	0.86	0.86	0.82	0.82	0.81
400	0.90	0.90	0.89	0.83	0.83	0.82	0.77	0.78	0.78
300	0.85	0.85	0.83	0.78	0.78	0.77	0.72	0.72	0.71
250	0.78	0.77	0.76	0.70	0.69	0.69	0.63	0.65	0.64
200	0.73	0.70	0.70	0.69	0.66	0.65	0.62	0.60	0.60
150	0.60	0.63	0.63	0.63	0.63	0.62	0.59	0.59	0.59
100	0.67	0.67	0.66	0.61	0.60	0.58	0.57	0.55	0.54

are reasonable and comparable to those in previous studies. Therefore, it is appropriate to utilize wetPf2 data which have higher temporal and spatial resolution than radiosonde station data for investigating the variability of temperature and relative humidity in the Paracel and Spratly regions, where operational radiosonde stations are currently unavailable.

3.2. Characteristics of the Temperature and Humidity Fields in Paracel and Spratly Islands Air Masses

3.2.1. Air temperature. Figure 4 illustrates the vertical profiles of the seasonal mean temperature (Tm) for the four seasons based on 6215 profiles of data in the Paracel region (13°N–18°N, 110°E–115°E). The results clearly depict the annual and vertical variations of the air mass temperature over the area. The temperature decreases gradually from the surface to the top of the troposphere (from 16.8 km to 17.5 km). The annual variation of Tm at each level follows a distinct pattern, with the highest values observed in summer and the lowest in winter. The Tm profile in the layer from 0 km to 3.5 km demonstrates relatively significant seasonal variations, with the amplitude of Tm variation ranging from 1.3°C to 5.0°C. Near the surface, Tm values are 24.0°C in winter and 28.5°C in summer. The large seasonal variation of Tm in lower levels may relate to the strong influence of the winter monsoon flow in this region. During winter, the winter monsoon brings cold air from the north, significantly lowering the temperature in this area compared to summer. Additionally, the effects of heating and near-surface turbulence lead to a much larger annual temperature variation in the boundary layer compared to the free atmosphere above. In the layer from 3.5 km to 16 km, Tm exhibits small seasonal variations.

The amplitude of Tm seasonal variation at different levels ranges from 0.4°C to 2.1°C. Above 16 km, the seasonal variation of Tm is larger than in the lower levels, with an amplitude ranging from 1.6°C to 5.8°C. The lowest Tm values are −83.1°C (in winter) and −79.4°C (in summer). These values are consistent with previous studies that stated the minimum temperature at the tropopause in the North Pacific monsoon region was about 194.0 K (−79.0°C) in summer and from 189.4 K to 190.6 K (−83.7°C to −82.5°C) in winter [19].

The vertical profiles of temperature (Tm) for the four seasons, derived from 7730 profiles of data in the Spratly Islands region, are presented in Figure 5. It indicates a similar variation trend of Tm with altitude as observed in the Paracel Islands region, decreasing gradually from the surface to the tropopause. Regarding the annual variability of Tm, in lower levels from the surface to 2.0 km, the highest values are found in summer, while the lowest values occur in winter. The amplitude of Tm seasonal variations at particular levels ranges from 1.2°C to 2.2°C. Near the surface, Tm values are 26.1°C (winter) and 28.3°C (summer). Compared with the Paracel region, the seasonal temperature variability in the Spratly Islands region is much smaller. This reflects the weaker influence of the winter monsoon winds in this region, resulting in higher winter Tm values and smaller

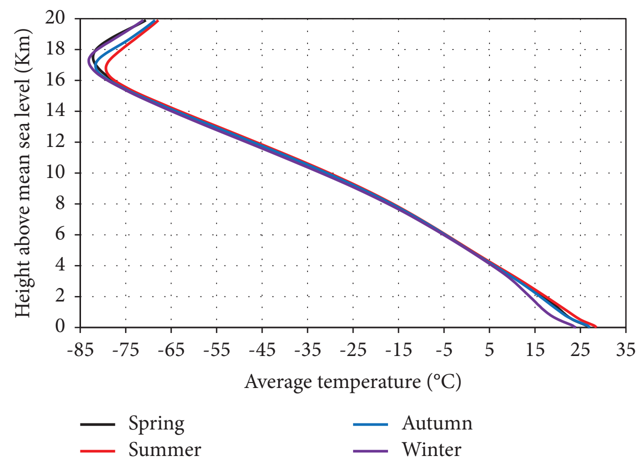

Figure 4: The average temperature profile of four seasons over the Paracel Islands region (13°N–18°N, 110°E–115°E).

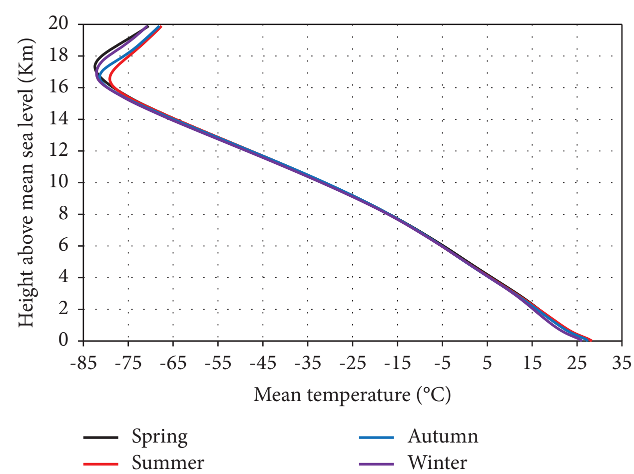

Figure 5: The average temperature profile of four seasons over the Spratly Islands region (07°N–12°N, 110°E–115°E).

temperature variations throughout the year over the Spratly Islands than over the Paracel region. From the 2.0 km to 15.8 km levels, Tm values are higher in spring compared to other seasons. The variations of Tm at particular levels within the layer are small seasonally dependent, with a variation amplitude ranging from 0.3°C to 1.4°C. In the upper atmosphere above 15.8 km, the highest Tm values are observed in summer. The amplitude of Tm variations at particular levels in this layer is larger than in the layer below, ranging from 1.4°C to 6.1°C. The minimum values of Tm are −79.1°C (summer) and −82.1°C (winter) (Figure 5).

To investigate the contrast in temperature between air masses in the north and south of the East Sea at different times of the year, Figure 6 presents the temperature differences with altitude between the air masses over the Paracel and Spratly regions during the summer (red line) and winter (blue line). The figure shows that in summer, the temperature difference between the two air masses is not significant (Figure 6). There is a noteworthy cooling effect (−1.0 to −2.3°C) in the lower atmosphere of the northern air

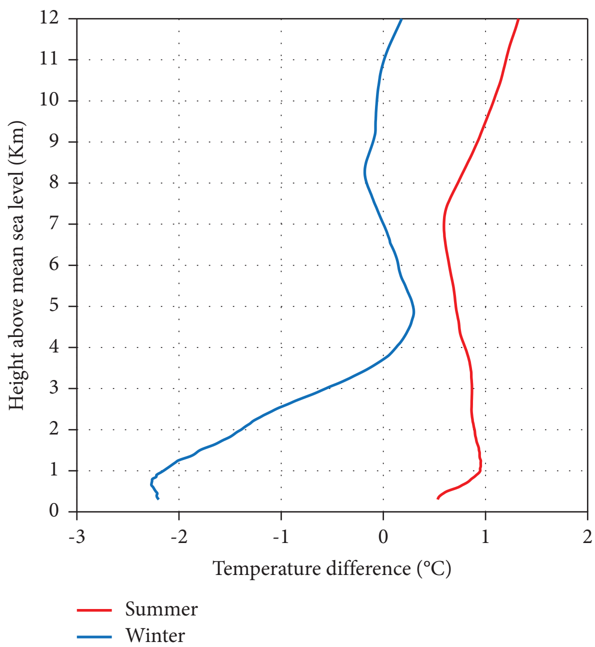

Figure 6: Vertical profile of temperature difference between two air masses over Paracel and Spratly Islands regions in summer (red) and winter (blue).

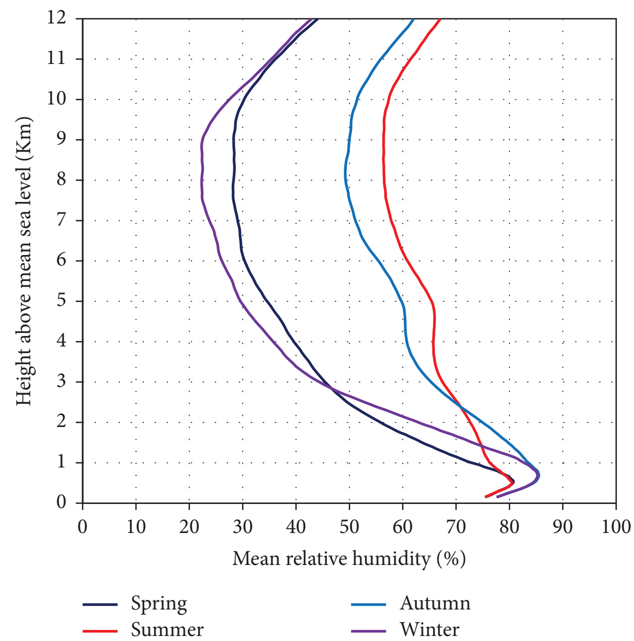

Figure 7: Average relative humidity profiles of four seasons over the Paracel Islands region (13°N–18°N, 110°E–115°E).

mass (above the Paracel Islands) compared to the southern air mass (above the Spratly Islands) during the winter season. The substantial temperature difference in winter is primarily influenced by the northward wind carrying cold air from higher latitudes to the Northern Vietnam and East Sea regions. Due to the characteristics of cold air in the region, which is mainly concentrated in the lower troposphere (below 3 km), the colder air mass over the northern part of the East Sea is predominantly concentrated at lower altitudes (below 3 km) (Figure 6).

3.2.2. Relative Humidity. Figure 7 represents the vertical profile of average relative humidity (RHm) in the range from 0 km to 12 km in the Paracel Islands region. The results show that the RHm values in the boundary layer are higher than in the free atmosphere layer. In the near-surface layer, the seasonal average humidity values range from 75.4% (summer) to 77.6% (winter). The RHm values increase with height and reach a maximum at around 0.6 km to 0.7 km. This height is often the location of the lifting condensation level (LCL). The maximum values of RHm are 80.7% in spring, 80.5% in summer, 85.5% in autumn, and 85.3% in winter. Due to the influence of winter monsoon winds, the cold air flow brings low-temperature air from the northern Asian continent to the East Sea, causing temperatures to approach the dew point. This results in the highest relative humidity values in this region during winter in the air layer from the surface to 400 m (Figure 7). In the free atmosphere layer, RHm decreases with height for spring, autumn, and winter, reaching a minimum value at the mid-tropospheric level, and then increases with height. However, for the summer RHm profile, a secondary maximum is observed at around 4.8 km. This secondary maximum value may be associated with the freezing level within convective clouds.

The amplitude of RHm variation with height is smallest in summer and largest in winter. The minimum values of RHm are 28.2% (spring), 56.4% (summer), 49.2% (autumn), and 22.3% (winter) at the 8 to 9 km level. The amplitude of the annual variation in RHm within the free atmosphere layer is much greater than in the boundary layer, reaching a maximum annual variation value of 35.8% (Figure 7). The RHm values in summer are significantly higher than in winter in the free atmosphere layer. The large decrease in humidity with height during winter, while relatively little variation in relative humidity occurs with height in summer, may be related to the important role of strong convective activity, which brings moist low-level air to higher atmospheric layers during summer.

Figure 8 represents the vertical profile of the average seasonal relative humidity (RHm) in the layer from 0 km to 12 km in the Spratly Islands region. The results show that the average seasonal humidity values range from 74.3% (summer) to 78.5% (winter) at the near-surface layer. Similar to the Paracel Islands region, the RHm values increase with altitude and reach a maximum at 0.65 km. The maximum values of RHm are 80.3% in spring, 81.6% in summer, 84% in autumn, and 85.4% in winter. Subsequently, RHm decreases gradually and reaches a minimum value in the middle troposphere. The RHm values in the boundary layer are higher than those in the free-atmosphere layer. In the layer below 1.25 km, the annual variation amplitude of RHm is small (<7.5%). Mean relative humidity has the highest values in winter. This may be due to the influence of winter monsoon winds and ITCZ (The Intertropical Convergence Zone) activities. The winter monsoon transports low-temperature air to the East Sea in combination with the

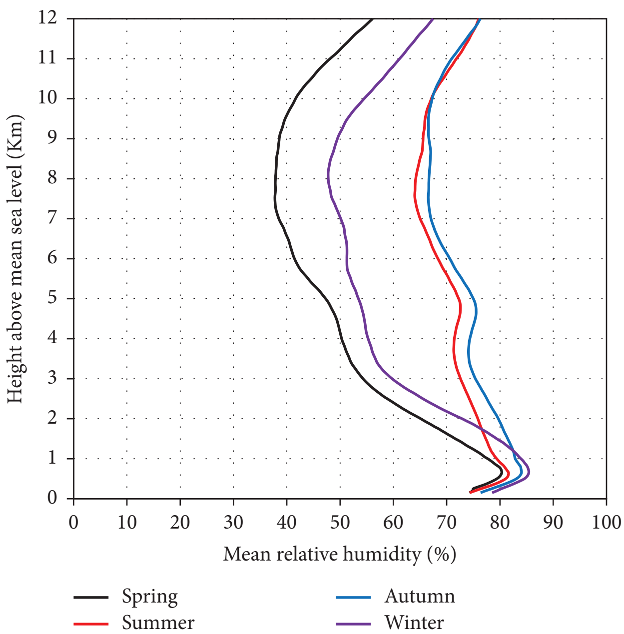

Figure 8: Average relative humidity profiles of four seasons over the Spratly Islands region (07°N–12°N, 110°E–115°E).

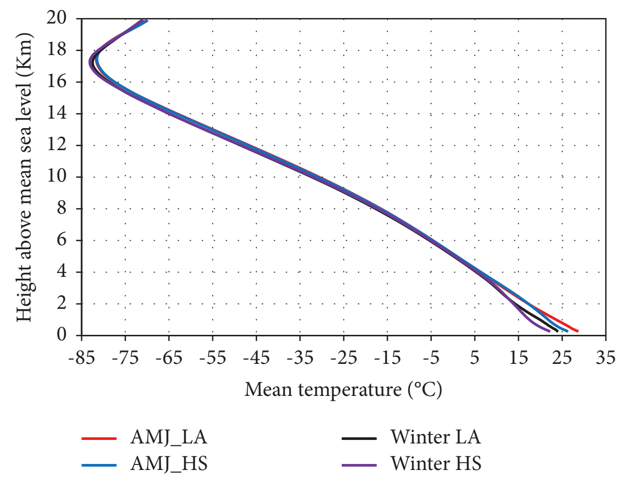

Figure 9: Average temperature profiles in hot months (AMJ) over land (red), over the sea (blue), and in winter (DJF) over land (black), and over the sea (purple).

ITCZ with active convection zone moving to lower latitudes (near and over the Spratly Islands region) in the early winter months. This results in high relative humidity within the air mass during the winter (Figure 8).

In the free atmosphere layer, RHm is higher in summer and autumn than in winter and spring. The amplitude of RHm variation with height in summer and autumn is smaller than that in winter and spring. The annual variation amplitude of RHm at the same altitude reaches a maximum value of 29.2% (Figure 8), which is smaller than that in the Paracel Islands region. The RHm values in summer and autumn do not significantly change with height in comparison to that in winter and spring. This feature may be related to the important role of strong convective activity in carrying moist low-level air to higher atmospheric layers during summer and autumn.

3.3. The Difference between the Temperature and Humidity Fields of Maritime Air Mass and the Continental Air Mass at the Same Latitude. To highlight the distinctive features of temperature and relative humidity variations over a maritime air mass, we compared the variations of the variables over the Paracel Islands region and that over the land area (13°N–18°N, 101°E–106°E). The land area region is chosen at the same latitudes as the maritime (the Paracel Islands) region. Based on surface station temperature statistics, the hottest temperatures over the land region occur in late spring to early summer [20]. The three-month period of April, May, and June (AMJ) is, therefore, selected to compute the mean temperature during the hot months. The winter period (DJF) is chosen to investigate the temperatures of the two air masses during the coldest months.

Figure 9 represents the average temperature profiles in April, May, and June (AMJ) and during winter over the land and the Paracel Islands areas. It shows that the average temperature profiles over the land area and the Paracel Islands area did not exhibit significant differences at higher levels (above 3 km). However, at lower levels (below 2 km) during the hot months (AMJ), the mean temperature of the land air mass is 1°C to 2°C higher than that in the maritime air mass due to heating over the land (Figure 9). The heating over land during the hot months can be observed more distinctly in Figure 10. Figure 10 displays the long-term (30 years) mean of 2 m air temperature and 10 m wind vectors from the ERA5 data. In April, the continental air mass exhibits noticeably higher air temperatures than the air mass over the Paracel Islands region (Figures 1 and 10). During the winter months, because the oceanic air mass is significantly influenced by cold air flow from the winter monsoon (Figure 11), the air temperature at lower levels of the land air mass remains 1°C to 2°C warmer than in the maritime air mass (Figures 1, 9, and 11).

Figure 12 represents the average relative humidity profiles in summer and winter over the land and the Paracel Islands areas. The results show that the amplitude of the annual relative humidity variation (summer RHm—winter RHm) is approximately 33.9% in the land air mass, which is much higher than in the maritime air mass (Figure 12).

In summer, the mean RHm values for both regions are high (Figure 12). Below 0.8 km, the RHm value of the maritime air mass is higher than that of the land air mass. The summer mean RHm of the air mass over the sea is higher in the lower part of the boundary layer, which may be associated with the role of turbulent motions that transport abundant moisture from the sea into the atmospheric boundary layer. However, in the free atmosphere layer, the summer mean RHm of the air mass over the land is higher than that over the Paracel Islands region (Figure 12). The reason may be that during the summer season, the southwest monsoon wind transports a moist air mass from the Indian Ocean to the mainland region [21]. Under the influence of local factors and topography, convection develops strongly, transporting moisture to higher levels in the free

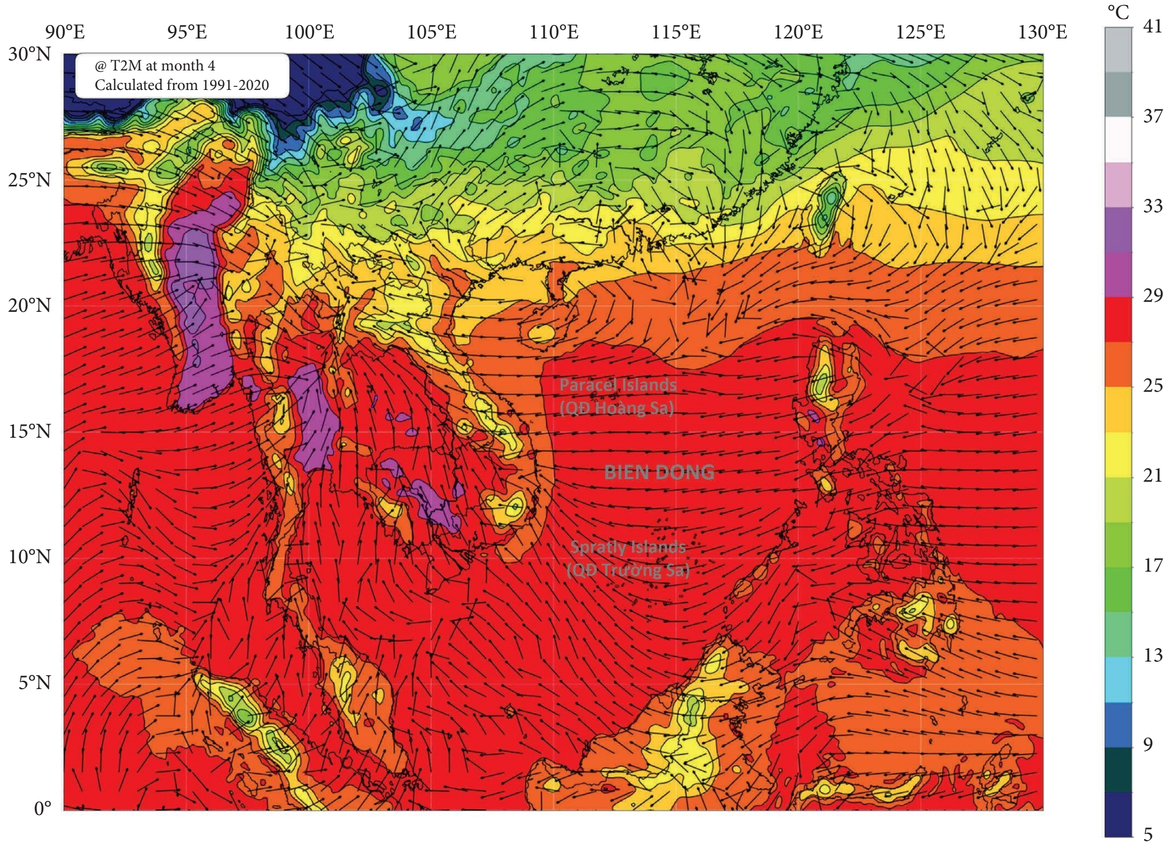

Figure 10: Long-term (1991–2020) mean of temperature (shaded, °C) and wind vectors (vector, m·s^{-1}) for April from ERA5 reanalysis data.

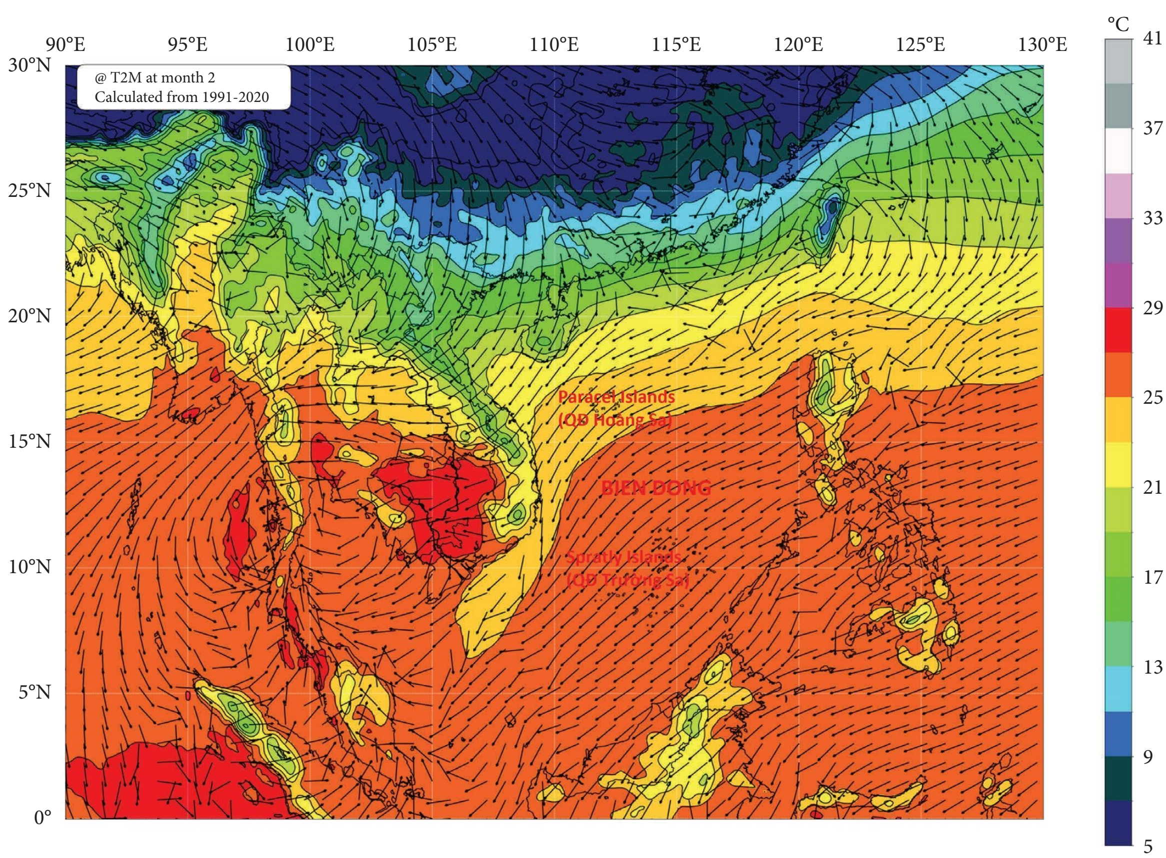

Figure 11: Long-term (1991–2020) mean of temperature (shaded, °C) and wind vectors (vector, m·s^{-1}) for February from ERA5 reanalysis data.

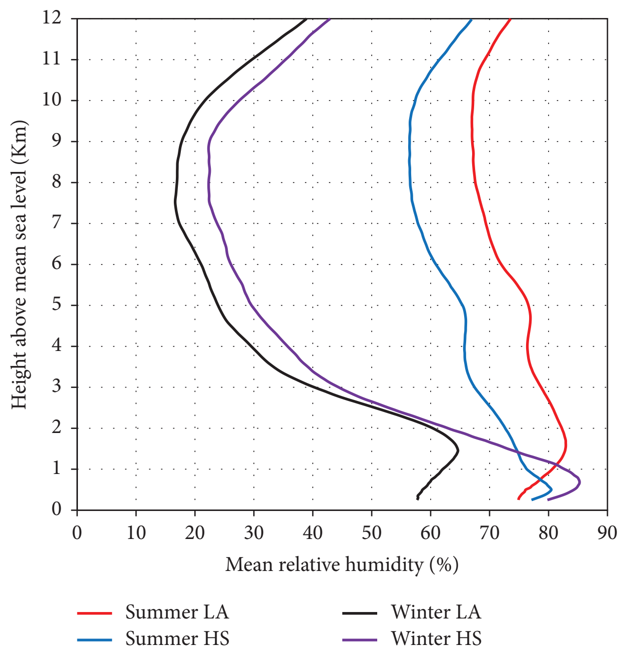

Figure 12: Average relative humidity (%) profile in summer (JJA) over land (red), over sea (blue), and in winter (DJF) over land (black), and over sea (purple).

atmosphere. This could be an important factor leading to higher RHm values over the land compared to the sea in the upper levels (above 1 km) in summer.

In winter, the average relative humidity profile exhibits a significant difference in the mean RHm of the two air masses within the atmospheric boundary layer (below 2 km). The RHm value over the land is much lower than that in the Paracel Islands region. During winter, the northeast monsoon brings a cool and dry air mass to this region [21]. Due to the influence of the dry northeast monsoon winds, the relative humidity of the air mass in the atmospheric boundary layer of this land area is lower than that in the Paracel Islands region. In the free atmosphere layer, the relative humidity values of the two air masses do not differ significantly, with a relatively lower value over the land area compared to the Paracel Islands region (Figure 12).

4. Summary and Discussion

This article utilizes data from the second-generation Constellation Observing System for Meteorology, Ionosphere, and Climate (COSMIC-2) satellites (wetPf2) to investigate the temperature and humidity properties of the air masses over the Paracel and Spratly Islands in the East Sea. The satellite observational data have been validated against radiosonde data from three stations in Vietnam: Hanoi, Danang, and Ho Chi Minh City. Subsequently, the wetPf2 data are employed to analyze the characteristics of temperature and relative humidity variations in the air masses over the regions of the Paracel and Spratly Islands.

The results show that the mean error of the satellite observational data for temperature ranges from −0.06°C to −0.02°C, with standard deviations ranging from 0.73°C to 1.04°C and correlation coefficients ranging from 0.86 to 0.93. The mean error of relative humidity fluctuates between 11.63% and 12.45%, with standard deviations ranging from 15.04% to 19.06% and correlation coefficients ranging from 0.63 to 0.76. The error statistics for the Vietnam region are consistent with those of previous studies. The results confirm that wetPf2 data are valuable for both research and operational applications in the region.

With a vertical resolution of 50 meters, the wetPf2 data provide detailed information on the vertical and seasonal variations of temperature and humidity over the Paracel and Spratly Islands. Specifically, the air mass over the Paracel Islands, representing the northern part of the East Sea, exhibits a larger annual temperature variation with an amplitude of approximately 5.0°C. This is significantly higher than the value of 2.2°C observed in the air mass over the Spratly Islands, representing the southern part of the East Sea. This difference may be attributed to the greater influence of continental and seasonal wind systems in the northern region. Due to the effects of heating and turbulent mixing near the Earth's surface, the annual temperature variation amplitude in the boundary layer is much larger than that in the free atmosphere.

The annual variation of relative humidity indicates higher RH values in summer and autumn compared to winter and spring. In the maritime boundary layer, the annual amplitude of relative humidity variation is small. Conversely, in the free atmosphere, relative humidity experiences a considerable annual amplitude variation. The maximum difference in RH between winter and summer is 35.83% in the Paracel area and 29.20% in the Spratly region.

The vertical variation of relative humidity shows peak RH values at heights of about 0.65 km over both the Paracel and Spratly Islands air masses, reaching a minimum in the mid-troposphere region. While there is a significant decrease in humidity with height during winter, no substantial change in relative humidity with height is observed during summer. The relatively smaller variation in relative humidity with height in the summer than in winter may be attributed to the crucial role of strong convective activities carrying moist air upward to higher atmospheric levels during the summer.

Data Availability

The data used to support the findings of this study are provided upon request or can be downloaded as following. (1) The wetPf2 data (COSMIC-2/FORMOSAT-7) from the Central Weather Administration (CWA) during a period of 4 years from October 2019 to September 2023 can be downloaded at https://tacc.cwa.gov.tw/data-service/fs7rt_tdpc/daily_tar/. (2) The RAOB data are obtained from the University of Wyoming at https://weather.uwyo.edu/upperair/sounding.html. (3) The 30 years of data (1991 to 2020) from the fifth generation of ECMWF (European Centre for Medium-Range Weather Forecasts) reanalysis, known as ERA5 can be downloaded at https://cds.climate.copernicus.eu.

Disclosure

Current affiliation: Northern Delta and Midland Regional Hydro-Meteorological Center, Vietnam Meteorology and Hydrology Administration, Ministry of Natural Resources and Environment, Hanoi, Vietnam.

Conflicts of Interest

The authors declare that there are no conflicts of interest regarding the publication of this paper.

Acknowledgments

This research was funded by the national project titled "Research on the Role of Cloud Physics Processes and Atmospheric-Ocean Interactions on the Track and Intensity of Typhoons in the East Sea and Forecasting Typhoon-Related Strong Winds and Heavy Rains over the Central Region" grand code: ĐTĐL.CN-90/21. The authors would like to express their gratitude to MSc. Tran Duy Thuc from the Institute of Meteorology, Hydrology, and Climate Change for assisting in creating Figures 10 and 11 for the paper. We also extend our thanks to the Taiwan Analysis Center for COSMIC for providing COSMIC-2 data. The authors also thank ECMWF and the University of Wyoming for providing ERA5 data and radiosonde data, respectively.

References

[1] R. Ware, C. Rocken, F. Solheim et al., "GPS sounding of the atmosphere from low Earth orbit: preliminary results," *Bulletin of the American Meteorological Society*, vol. 77, no. 1, pp. 19–40, 1996.

[2] E. R. Kursinski, G. A. Hajj, J. T. Schofield, R. P. Linfield, and K. R. Hardy, "Observing earth's atmosphere with radio occultation measurements using the Global Positioning System," *Journal of Geophysical Research: Atmospheres*, vol. 102, no. D19, pp. 23429–23465, 1997.

[3] J. Wickert, T. Schmidt, G. Beyerle, R. König, C. Reigber, and N. Jakowski, "The radio occultation experiment aboard CHAMP: operational data analysis and validation of vertical atmospheric profiles," *Journal of the Meteorological Society of Japan*, vol. 82, no. 1B, pp. 381–395, 2004.

[4] T. Schmidt, S. Heise, J. Wickert, G. Beyerle, and C. Reigber, "GPS radio occultation with CHAMP and SAC-C: global monitoring of thermal tropopause parameters," *Atmospheric Chemistry and Physics*, vol. 5, no. 6, pp. 1473–1488, 2005.

[5] G. Beyerle, T. Schmidt, G. Michalak, S. Heise, J. Wickert, and C. Reigber, "GPS radio occultation with GRACE: atmospheric profiling utilizing the zero difference technique," *Geophysical Research Letters*, vol. 32, no. 13, 2005.

[6] R. A. Anthes, P. A. Bernhardt, Y. Chen et al., "The COSMIC/FORMOSAT-3 mission: early results," *Bulletin of the American Meteorological Society*, vol. 89, no. 3, pp. 313–334, 2008.

[7] M. E. Gorbunov, K. B. Lauritsen, H.-H. Benzon, G. B. Larsen, S. Syndergaard, and M. B. Sørensen, "Processing of GRAS/METOP radio occultation data recorded in closed-loop and raw-sampling modes," *Atmospheric Measurement Techniques*, vol. 4, no. 6, pp. 1021–1026, 2011.

[8] W. S. Schreiner, J. Weiss, R. Anthes et al., "COSMIC-2 radio occultation constellation: first results," *Geophysical Research Letters*, vol. 47, no. 4, p. 2020, 2020.

[9] K. Zhang, E. Fu, D. Silcock, Y. Wang, and Y. Kuleshov, "An investigation of atmospheric temperature profiles in the Australian region using collocated GPS radio occultation and radiosonde data," *Atmospheric Measurement Techniques*, vol. 4, no. 10, pp. 2087–2092, 2011.

[10] Y. Kuleshov, S. Choy, E. Fu, F. Chane-Ming, Y. A. Liou, and A. G. Pavelyev, "Analysis of meteorological variables in the Australasian region using ground- and space-based GPS techniques," *Atmospheric Research*, vol. 176-177, pp. 276–289, 2016.

[11] G. Xu, X. Yue, W. Zhang, and X. Wan, "Assessment of atmospheric wet profiles obtained from COSMIC radio occultation observations over China," *Atmosphere*, vol. 8, no. 11, p. 208, 2017.

[12] B. Sun, A. Reale, D. J. Seidel, and D. C. Hunt, "Comparing radiosonde and COSMIC atmospheric profile data to quantify differences among radiosonde types and the effects of imperfect collocation on comparison statistics," *Journal of Geophysical Research: Atmospheres*, vol. 115, no. D23, 2010.

[13] B. R. Wang, X. Y. Liu, and J. K. Wang, "Assessment of COSMIC radio occultation retrieval product using global radiosonde data," *Atmospheric Measurement Techniques*, vol. 6, no. 4, pp. 1073–1083, 2013.

[14] S.-P. Ho, X. Zhou, X. Shao et al., "Initial assessment of the COSMIC-2/FORMOSAT-7 neutral atmosphere data quality in NESDIS/STAR using in situ and satellite data," *Remote Sensing*, vol. 12, no. 24, p. 4099, 2020.

[15] X. Shao, S.-P. Ho, B. Zhang et al., "Comparison of COSMIC-2 radio occultation retrievals with RS41 and RS92 radiosonde humidity and temperature measurements," *Terrestrial, Atmospheric and Oceanic Sciences*, vol. 32, no. 6.1, pp. 1015–1032, 2021.

[16] V. Veenus, S. S. Das, B. Sama, and K. N. Uma, "A comparison of temperature and relative humidity measurements derived from COSMIC-2 radio occultations with radiosonde observations made over the Asian summer monsoon region," *Remote Sensing Letters*, vol. 13, no. 4, pp. 394–405, 2022.

[17] Y.-C. Chen, C.-C. Tsai, Y.-C. Wu et al., "Evaluation of operational monsoon moisture surveillance and severe weather prediction utilizing COSMIC-2/FORMOSAT-7 radio occultation observations," *Remote Sensing*, vol. 13, no. 15, p. 2979, 2021.

[18] Q. N. Pham, V. K. Mai, Q. T. Nguyen, and V. T. Vu, "An experiment with GSI for data assimilation to improve quantitative rainfall forecast over Southern Vietnam region," *Vietnam Journal of Hydro Meteorology*, vol. 698, pp. 1–10, 2019.

[19] E. Nishimoto and M. Shiotani, "Seasonal and interannual variability in the temperature structure around the tropical tropopause and its relationship with convective activities," *Journal of Geophysical Research: Atmospheres*, vol. 117, no. D2, 2012.

[20] P. Senapeng, T. Prahadchai, P. Guayjarernpanishk, J.-S. Park, and P. Busababodhin, "Spatial modeling of extreme temperature in northeast Thailand," *Atmosphere*, vol. 13, no. 4, p. 589, 2022.

[21] J. Khedari, A. Sangprajak, and J. Hirunlabh, "Thailand climatic zones," *Renewable Energy*, vol. 25, no. 2, pp. 267–280, 2002.